Doped Sol-gel TiO_2 Films for Biological Applications

M. Gartner,[*] C. Trapalis,[†] N. Todorova,[†] T. Giannakopoulou,[†] G. Dobrescu, M. Anastasescu, P. Osiceanu, A. Ghita, M. Enache,[‡] L. Dumitru,[‡] T. Stoica,[§] M. Zaharescu, J. Y. Bae,[#] and S.-H. Suh[#,*]

Institute of Physical Chemistry, "Ilie Murgulescu", Romanian Academy, Bucharest 060021, Romania
[*]E-mail: mfgartner@yahoo.com
[†]Institute of Materials Science, National Center for Scientific Research, Athens, Greece
[‡]Institute of Biology, Center of Microbiology, Bucharest, Romania
[§]National Institute of Materials Physics, Bucharest, Romania
[#]Department of Chemistry and Chemical Engineering, Keimyung University, Daegu 704-701, Korea. [*]E-mail: shsuh@kmu.ac.kr
Received November 6, 2007

Mono and multilayer TiO_2(Fe, PEG_{600}) films were deposited by the dip-coating on SiO_2/glass substrate using sol-gel method. In an attempt to improve the antibacterial properties of doped TiO_2 films, the influence of the iron oxides and polyethilenglycol (PEG_{600}) on the morphological, optical, surface chemical composition and biological properties of nanostructured layers was studied. Complementary measurements were performed including Spectroscopic Ellipsometry (SE), Scanning Electron Microscopy (SEM) coupled with the fractal analysis, X-Ray Photoelectron Spectroscopy (XPS) and antibacterial tests. It was found that different concentrations of Fe and PEG_{600} added to coating solution strongly influence the porosity and morphology at nanometric scale related to fractal behaviour and the elemental and chemical states of the surfaces as well. The thermal treatment under oxidative atmosphere leads to films densification and oxides phase stabilization. The antibacterial activity of coatings against Escherichia Coli bacteria was examined by specific antibacterial tests.

Key Words : Sol-gel, Doped TiO_2 thin films, SE, XPS, Antibacterial tests

Introduction

Titanium dioxide (TiO_2) is well-known as having a relatively wide band gap, 3.2 eV[1-4] and a high refractive index.[5-7] It is recognized as the most efficient photocatalytic material, but, due to its large band gap energy, it can only be excited by UV irradiation. However, doping TiO_2 with transitional metals represents a promising modification method for the utilization of visible light in photocatalysis.[8,9] Much effort is paid to its use for the photo-assisted degradation of bacteria and organic molecules. After irradiation in UV-visible, electron-hole pairs are created and separated such as the resulted free charge carriers might migrate to the surface. The reactive species may interact with adsorbed water and oxygen to produce radical species attacking the adsorbed organic molecules, bacteria and tumor cells.[10]

In recent years the sol-gel method has been widely used to prepare thin and thick films with well defined properties such as controlled refractive index, tailored chemical composition, crystallinity, porosity, particle size, degree of homogeneity, etc. By introducing porosity into the low refractive index coatings and keeping under control the interface composition, it would be possible to deposit sequential layers with great differences in the refractive index or with a controlled gradient.[11]

The aim of this work is the study of the influence of iron oxides and PEG_{600} on the morphological, optical, chemical surface composition and antibacterial properties of nanostructured TiO_2 films.

Experimental Section

Films preparation. TiO_2(Fe, PEG_{600}) films were deposited on SiO_2/glass substrates by dipping, from a sol-gel solution obtained by the hydrolysis of metal alkoxides in alcoholic medium and in the presence of acid catalysts.[12] More details can be found in our previous works.[13,14] The precursors were $Ti(OC_4H_9)_4$ as TiO_2 source and $Fe(NO_3)_3{\cdot}9H_2O$ as iron source and the molar ratio of the reagents was: $Ti(OC_4H_9)_4/C_2H_5OH/H_2O/HNO_3$ = 1:26.5:1.35:0.35, respectively. The densification of the film was performed by the thermal treatment in the conditions presented in the Table 1.

The following type of samples were prepared:

a) films with 7 wt % iron and different quantity of PEG_{600}, as listed in Table 1,

b) films with 1-5 stacks (where every stack is composed by 3 layers), containing different PEG_{600} concentrations.

Table 1. Experimental details of the TiO_2 (7%Fe, PEG_{600}) films as prepared and thermally treated in oxidative atmosphere

Sample	PEG_{600} (M)	Layers number	T (°C)	t (min)
121x	0	1	as prepared	
121y	0.017	1	500	30
121z	0.035	1	500	30
121e3F	0.069	3	500	30
121a3F	0.139	3	500	30
121b3F	0.278	3	500	30

Table 2. Composition of the investigated film coatings in antibacterial tests

Sample No.	Fe (%)	PEG_{600} (M)	Time of Thermal Treatment (h)
1	1.23	0.060	1
2		0.029	
3		0.014	
4		0.110	
5		0	
6	7	0.069	3
7		0.017	
8	Glass sample, free of coatings		

These films present refractive index gradient in the bulk. The most complex one (P4 which has 5 stacks) has the following composition:

SiO_2/3 layers 121x/3 layers 121y/3 layers 121z/3 layers 121e/3 layers 121(a)

c) films with 1.23 wt % iron and different quantity of PEG as is listed in Table 2

Film characterization. The optical properties of as-prepared and annealed films were determined by spectroellipsometric (SE) measurements in the visible spectral range (0.4-0.7 μm). The morphology of the surface was obtained by SEM measurements, using a JEOL field emission scanning electron microscope. Fractal dimensions of the films were computed using SEM micrographs and the correlation function together with the variable length scale methods. The XPS elemental and chemical surface analysis was performed by a VG ESCA 3 spectrometer pumped down to 10^{-9} Torr and using AlKα radiation (1486.6 eV) with an energy overall resolution of 1.2 eV. Energy calibration has been carried out by using the internal standard C1s photoelectron line at 284.6 eV from adventitious hydrocarbon. All the XPS spectra have been recorded without Ar sputtering. The antibacterial tests were carried out by (i) the evidence of the inhibitory effect against *E. coli* growth (depending on coating films composition) and (ii) the influence of coatings composition on the adherence of *E. coli* to the films surface. The *E. coli* was cultivated in the presence of tested samples for 72 hours at 37 °C in flasks containing 22.5 mL broth and 2.5 ml bacterial inoculum. The inhibitory effect of coatings composition on the growth of *E. coli* was evaluated by reading optical density at 660 nm. The coating compositions employed for these experiments are listed in Table 2.

Results and Discussion

The obtaining of the refractive index, n, and the thickness of the films from ellipsometric measurements ware performed using the Bruggemann Effective Medium Approximation (B-EMA).[15] For the most complex sample, P4, we used the model with 5 layers on the SiO_2/glass with the following components: amorphous-TiO_2, anatase, Fe_2O_3 and voids having different relative ratios on each layer. Since PEG_{600} was decomposed and removed from the film matrix after thermal treatment, the content of PEG_{600} in the film was simulated with voids. Refractive index, n, for every layer obtained from the best fit is shown in Figure 1. and the extinction coefficients, k, were found to be zero. Since the number of the thermal treatments varies for each layer as well as the PEG_{600} content, the refractive index values differ consequently, leading to the gradient of refractive index along the bulk of the sample. The total thickness of the film obtained by summing the thickness of each layer was found 389 ± 3 nm. The porosity of each three layer stack lied in the range of 5-22% volumic fractions giving rise to different refractive indices as shown in Figure 1.

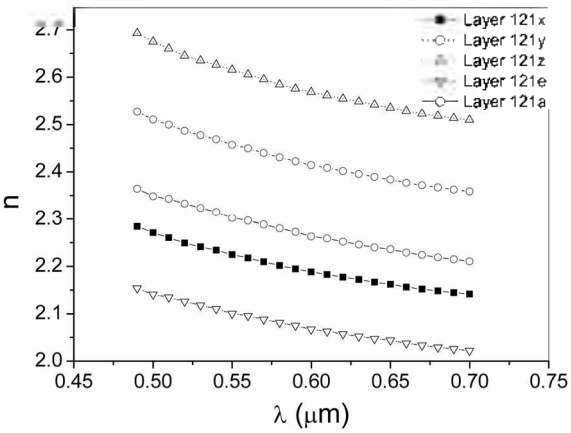

Figure 1. Refractive index dispersions for each layer of the sample P4.

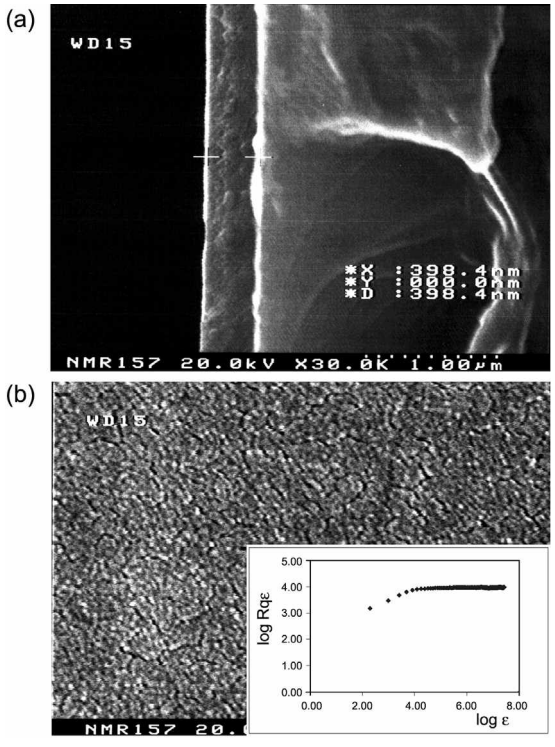

Figure 2. SEM images on sample P4. (a) cross section view with the value of the thickness and (b) plan view; the inserted graph represents the log-log plot of root-mean-square deviation $R_{q\varepsilon}$ versus the interval length ε from the variable length scale method.

In the Figure 1 the curve for fresh sample 121x is the spectrum of the one layer "as prepared film" and it is reasonable to have the refractive index lower than the refractive indices of the films treated at high temperatures. In the same figure the curves of one layer films 121y and 121z show a higher refractive index because the addition of PEG_{600} in low quantity contributes to enhance the sol-gel process leading to formation of thicker coating which during densification at 500 °C leads to denser films. In the case of layers 121e and 121a due to higher PEG_{600} content, an advanced densification was not possible during the thermal treatment and films with bigger porosity were generated.

SEM analysis was carried out in order to check the thickness value obtained by spectroellipsometry (SE), and also to determine the average grain size of the particles in the films. One can notice in Figure 2a that the thickness of the films obtained by SE fitting (d = 389 nm) is very close to the value obtained by SEM (398.4 nm). Therefore, we conclude that the SE fitting model used in this work is appropriate to describe the optical dispersion relation of the films. Grain size was estimated to be in the range of 15-35 nm as can be seen in Figure 2b. From SEM micrographs it can be observed a very good adherence of the film on the substrate, the high degree of homogeneity and the low level of roughness.

Fractal analysis of SEM images of the TiO_2 samples with 0.035 M and 0.278 M PEG_{600} in Figures 3a and 3b shows that the corresponding surface is self-similar for a large scaling domain. Thus, the 0.035 M PEG_{600} sample is characterized by the fractal dimension of 2.63 ± 0.02, the linear correlation coefficient 0.990 and the scaling ranges of 30-270 nm (Figure 3a). The increasing of PEG_{600} content (the sample with 0.278 mol PEG_{600}) leads to the higher fractal dimension of 2.89 ± 0.01, the linear correlation coefficient 0.973 and the cut-offs limits 5-164 nm (Figure 3b). The higher fractal dimension indicates the higher surface corrugation as the result of increasing porosity due to the larger amount of PEG_{600} used. Image analysis of SEM micrograph for the five-layers TiO_2 film (P4 sample) presented in Figure 2b shows a self-similar surface characterized by the bi-modal fractal behaviour. Therefore, the structure is characterized by two fractal dimensions; for the lower self-similarity domain (5-25 nm), the fractal dimension of 2.56 ± 0.02 was obtained with a linear correlation coefficient of 0.995, while, for the intermediate self-similarity domain (25-46 nm), the fractal dimension of 2.88 ± 0.01 was evaluated.

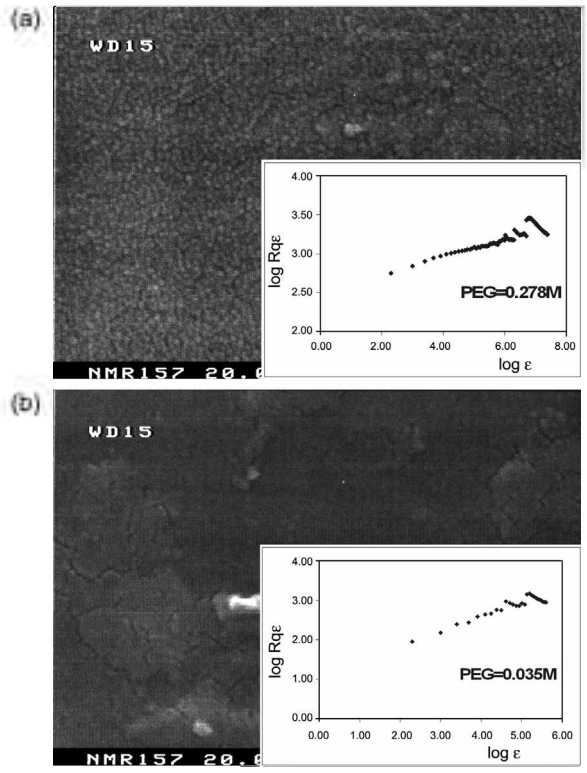

Figure 3. (a) SEM micrograph and fractal analysis of the TiO_2 film prepared with 0.278 M PEG_{600} deposited on a SiO_2/glass substrate, and (b) SEM micrograph and fractal analysis of the TiO_2 film prepared with 0.035 M PEG_{600} deposited on a SiO_2/glass substrate.

While the one layer samples analysed, as observed in Figures 3a and 3b, were characterized by a single fractal dimension and a large self-similarity domain, the multilayer sample is characterized by two narrow self-similarity domains and two different fractal dimensions. The bi-modal behaviour is related to PEG_{600} concentration depth-profile of the analysed sample. According to these results, the fractal dimension increases with PEG_{600} concentration as result of increasing porosity. The layers with increasing fractal dimensions were found to be characterized by bi-modal fractal behaviour and narrow self-similarity domains. The fractal dimension value of 2.88 obtained here is close to the fractal dimension of the 0.278 moles PEG_{600} film (2.89 ± 0.01). We can expect this fractal dimension to characterize the top layer (the 0.139 M PEG_{600} layer); the fractal dimension of 2.56 is the result of successive deposited layers, and it is an overall characteristic of the inner layers with PEG_{600} concentrations between 0 and 0.069 M.

XPS analysis was used to determine the elemental relative concentrations for titanium and iron oxides. After spectra deconvolution the following results were found out:

(i) Titanium is full oxidized (4+ oxidation state) for all samples showing the characteristic 2p3/2 and 2p1/2 photoelectron lines at 458.7 eV and 464.5 eV, respectively (see Figure 4a).

(ii) Iron oxides reveals the different and more complicated pattern as a result of the hybridization between Fe3d and the ligand O2p orbitals, giving rise to multiplet structures in the spectra. Thus, for the "as prepared" sample, the 2p photoelectron doublet exhibits the characteristic structure of the 2+ oxidation state both in binding energy assignment and the satellite structure. The binding energies for the main photoelectron lines are as follows: 2p3/2 line at 709.7 eV, 2p1/2 line at 723.2 eV, and the corresponding satellite lines at 714.7 eV and 729.8 eV, respectively. The result in Figure 4b can be the fingerprint to identify almost unambiguously the 2+ oxidation state.[16,17]

However, the mixture of (2+, 3+) oxidation states cannot be completely ruled out, but in this case, the most prominent state remains 2+. The reduction of the Fe^{3-} from the iron-

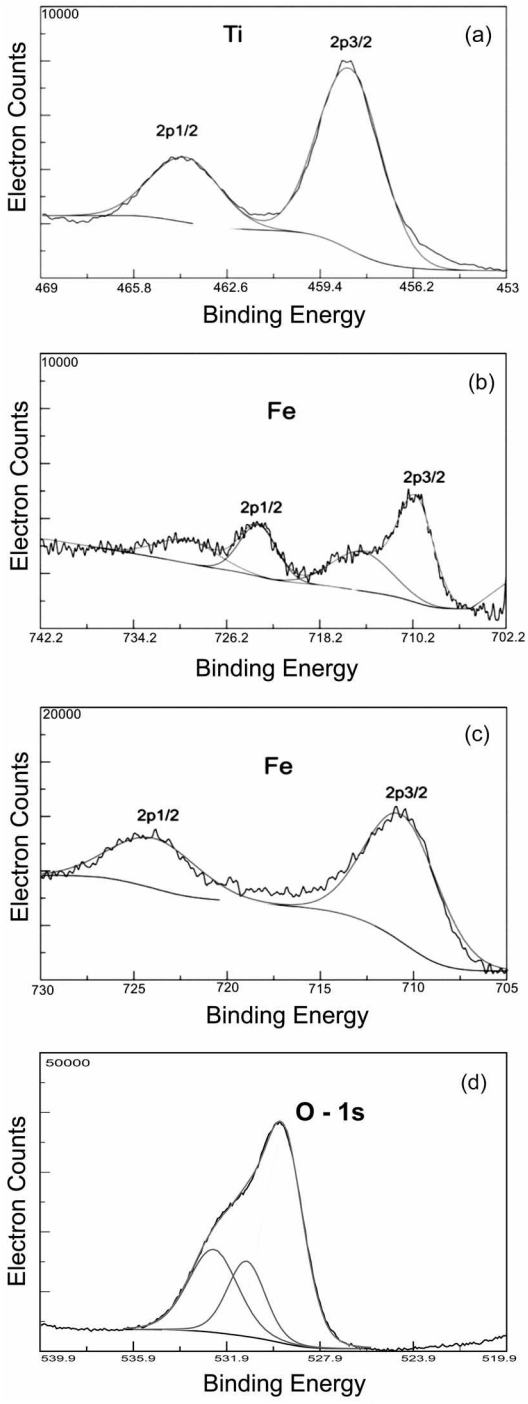

Figure 4. (**a**) Ti 2p photoelectron spectrum for the sample 121z, (**b**) Fe 2p photoelectron spectrum for the sample121x, (**c**) Fe 2p photoelectron spectrum for the sample 121z, (**d**) O1s deconvoluted photoelectron spectrum for the sample 121z.

precursor to Fe^{2-} could occur during the sol-gel process that take place in the alcoholic solutions. After heating the samples at 500 °C under oxygen atmosphere, the iron oxide (FeO) undergoes a change to Fe_3O_4 (magnetite) which is the mixed-valence compound with Fe^{2+} ions occupying octahedral sites and Fe^{3+} being distributed between octahedral and tetrahedral sites according to the structural formula: $[Fe^{3+}]_{tet}$-$[Fe^{2+}/Fe^{3+}]_{oct}O_4$. The assignments of the binding energies

Table 3. Surface stoichiometry obtained by XPS analysis

Sample	Stoichiometric formula
121x	$Fe_{0.16}Ti_{0.84}O_y$
121z	$Fe_{0.11}Ti_{0.89}O_y$
121a	$Fe_{0.10}Ti_{0.90}O_y$
121b	$Fe_{0.11}Ti_{0.89}O_y$

(2p3/2 line at 710.9 eV and 2p1/2 line at 724.5 eV) as well as the general shape of the spectrum, *i.e.*, the characteristic satellites strongly smeared-out and an asymmetric broadening of the Fe2p main peaks that can be noticed in Figure 4c, lead to the conclusion that the oxide obtained is Fe_3O_4.[16,18] Except for the "as prepared" sample, oxygen is found to be in excess in the oxidized samples, suggesting its incorporation into interstitial sites and/or occupying some vacancies left by Fe^{2-} ions into octahedral sites in some possible nonstoichiometric oxides such as $Fe_{3-\delta}O_4$.

For fitting O1s peak we kept the value of Fe-O bonding at the fixed value of 530.1 eV for all the oxidation states of Iron as it is reported by Fujii *et al.*[16] Besides the Ti-O bonding in TiO_2, some other bondings are related to carbon as C-O and OH-C=O. As can be noticed from Figure 4d, from lower to higher binding energies (BS's) the first peak exhibits the oxygen bonded in TiO_2, the second is related on iron oxides and the last contribution is assigned to the adsorbed OH groups, water and OH-C-O bondings.

The quantitative analysis has shown a large amount of carbon present on the surface of the "as prepared" sample (55%) from adsorbed hydrocarbon, in particular from incomplete burning of the precursors. After oxidative treatments the carbon relative concentrations decrease to around 29%. After carbon removal we proceeded with data processing to obtain the surface stoichiometry starting from the intended bulk one: $Fe_{0.13}Ti_{0.87}O_y$. The results are presented in Table 3. Within experimental and fitting errors the "bulk" stoichiometry is in good agreement with the surface ones. However, a slight excess of iron in the "as prepared" sample suggests that the iron has not been completely transferred into the matrix.

In order to make a systematic study regarding the antibacterial activity of TiO_2(Fe. PEG_{600}), the films with 7% iron, prepared in the present work, were compare with films with lower iron content, 1.23 wt % and different PEG_{600} amount (see in Table 2). The results indicate the antibacterial activity of film coatings according to their composition. At the iron concentration of 1.23% (samples 1 to 5), the inhibitory effect is influenced by PEG_{600} concentrations, and the intensity of the effect is smaller as PEG_{600} concentration increases, except for the sample 1 (0.06 M PEG_{600} concentration). The absence of PEG_{600} from coating composition (sample 5) leads to a lower inhibitory effect as compared with sample 1 (0.06 M PEG_{600}). Increasing iron concentrations at 7% (samples 6 and 7) shows an enhancement of the inhibitory effect at the same PEG_{600} concentration (0.01 M in sample 3 and 7). For the same iron concentration of 7%, the increasing of PEG_{600} amount to 0.069 M (sample 6)

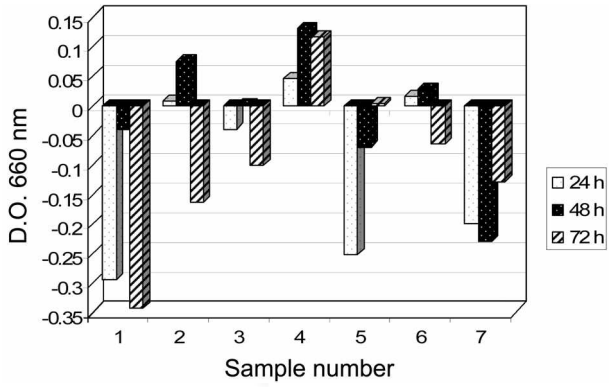

Figure 5. The inhibitory effect of film compositions on the *E. coli* growth.

determines the decreasing of inhibitory effect.

Growth of *E. coli* strain in the presence of different film composition reveals an inhibitory effect depending on PEG_{600} and Fe concentration, as can be seen in Figure 5. From these results an optimum concentration of PEG_{600} (0.017 M) for the inhibitory effect can be noticed. The influence of PEG_{600} can be slowly reduced by increasing Fe concentration until to 7% (see in Figure 5 for sample 7).

It should be assumed that high concentration of iron have an inhibitory effects towards the enzymatic equipment involved in essential metabolic pathways and in this way help to increase inhibitory effect of investigated films. Polyethylene glycol in high concentration conducted to increase porosity of films and then enhancing the possibility of bacterial cells for adhesion and growth at film surface. In this way presence of PEG_{600} higher that 0.01 M argue for antibacterial properties decreasing.

Conclusions

In the present work the two type of TiO_2(Fe.PEG_{600})/SiO_2/glass films were prepared with the different amount of PEG_{600}. From SEM images the grain size of nanoparticles was found in the range of 15-35 nm and the fractal analysis has proved the self-similarity of the surfaces on a large scale domain and the bi-modal fractal behaviour for the sample with the refractive index gradient in the bulk. From XPS analysis the presence of Fe^{2-} in the 'as prepared' sample was identify; by oxidation process a mixture of 2+/3+ valence states in Fe_3O_4 was determined. The inhibitory effect of *E. coli* growth depends on PEG_{600} and Fe concentration. The antibacterial tests show that the high concentration of PEG_{600} argues against the inhibitory effect. The influence of PEG_{600} can be slowly reduced with increasing Fe concentration up to 7%.

Acknowledgements. One of the authors (M. Gartner) wishes to acknowledge for the financial support of the EU Transactional Access Program, under the RIMDAC scheme at the NMRC, University College Cork, Ireland. The financial support of CEEX research contract (318/2006-2008) and MOCIE (No. RT104-03-02) are also gratefully acknowledged.

References

1. Kasikov, A.; Aarik, J.; Mandar, H.; Moppel, M.; Pars, M.; Uustare, T. *J. Phys. D: Appl. Phys.* **2006**, *39*, 54.
2. Tang, H.; Prasad, K.; Sanjines, R.; Schmid, P. E.; Levy, F. *J. Appl. Phys.* **1994**, *75*, 2042.
3. Dannenberg, R.; Greene, P. *Thin Solid Films* **2000**, *360*, 122.
4. Rodrigues, J.; Gomez, M.; Ederth, J.; Niklasson, G. A.; Granqvist, C. G. *Thin Solid Films* **2000**, *365*, 119.
5. Mitchell, D. R. G.; Attard, D. J.; Finnie, K. S.; Triani, G.; Barbe, C. J.; Depagne, C.; Barlett, J. R. *Appl. Surf. Sci.* **2005**, *243*, 265.
6. Zaitsu, S.; Motokoshi, S.; Jitsuno, S.; Nakatsuka, M.; Yamanaka, T. *Japan J. Appl. Phys.* **2002**, *41*, 160.
7. Aarik, J.; Aidla, A.; Mandar, H.; Uustare, T.; Schuisky, T.; Harsta, A. *J. Cryst. Growth* **2002**, *242*, 189.
8. Linsebigler, A. L.; Lu, G.; Yates Jr., J. T. *Chem. Rev.* **1995**, *95*, 735.
9. Hoffman, H.; Martin, S.; Choi, W.; Bahnemann, D. *Chem. Rev.* **1995**, *95*, 69.
10. Diebold, U. *Surf. Sci. Rep.* **2003**, *48*, 53.
11. Yan, Y.; Chaudhuri, S. R.; Chen, D.-G.; Sarkar, A. *Chem. Mater.* **1996**, *7*, 2007.
12. Chrysicopoulou, P.; Davazoglou, D.; Trapalis, C.; Kordas, G. *Thin Solid Films* **1998**, *323*, 188.
13. Trapalis, C. C.; Keivanidis, P.; Kordas, G.; Zaharescu, M.; Crisan, M.; Szatvanyi, A.; Gartner, M. *Thin Solid Films* **2003**, *433*, 186.
14. Trapalis, C.; Gartner, M.; Kordas, G.; Anastasescu, M.; Zaharescu, M.; Modreanu, M. *Appl. Surf. Sci.* (in press)
15. Bruggeman, D. G. A. *Ann. Phys. (Leipzig)* **1935**, *24*, 636.
16. Fujii, T.; De Groot, F. M. F.; Sawatzky, G. A. *Phys. Rev. B* **1999**, *59*, 3195.
17. *Handbook of X-Ray Photoelectron Spectroscopy*; Muilenberg, G. E., Ed.; Perkin-Elmer Corporation: Minnesota, 1979.
18. Wang, L.; Luo, J.; Fan, Q.; Suzuki, M.; Suzuki, I. S.; Engelhard, M. H.; Lin, Y.; Kim, N.; Wang, J. Q.; Zhong, C.-J. *J. Phys. Chem. B* **2005**, *109*, 21593.